

Supernova Neutrino Decoupling Is Altered by Flavor Conversion

Shashank Shalgar ¹ and Irene Tamborra ¹

¹*Niels Bohr International Academy & DARK, Niels Bohr Institute,
University of Copenhagen, Blegdamsvej 17, 2100 Copenhagen, Denmark*

(Dated: June 3, 2022)

The large neutrino density in the deep interior of core-collapse supernovae makes neutrino flavor evolution non-linear because of the coherent forward scattering of neutrinos among themselves. Under the assumption of spherical symmetry, we model neutrino decoupling from matter and present the first non-linear simulation of flavor evolution in the presence of charged current and neutral current collisions and neutrino advection. Flavor transformation occurs before neutrinos are fully decoupled from matter, dynamically affecting the flavor distributions of all neutrino species and shifting the location of the neutrino decoupling surfaces. Our findings may have implications on the explosion mechanism of supernovae, the nucleosynthesis of the heavy elements, as well as the observable neutrino signal, all of which is yet to be assessed.

Introduction.—Neutrinos are fundamental particles in the physics of core-collapse supernovae [1, 2]. Neutrinos are copiously emitted as matter accretes onto the proto-neutron star and transport energy and lepton number. According to the delayed neutrino-driven mechanism [3–5], neutrinos are essential to revive the stalled shock wave, powering the explosion.

Despite swift progress occurring in the last decade, not all supernova hydrodynamic simulations explode in three dimensions, hinting that crucial physics could be missing [1, 2, 6, 7]. For example, neutrinos are treated as radiation in hydrodynamic simulations [8]. However, they should be modeled through a quantum kinetic approach describing the evolution of the distributions of all six neutrino species (three neutrino flavors and their antiparticles), including flavor mixing [9–13]. This approximation is adopted because solving the full quantum kinetic transport of neutrinos is a formidable task, entailing the solution of a 7-dimensional non-linear problem (involving time, three spatial coordinates, energy, and two angular degrees of freedom), whose characteristic quantities rapidly vary by many orders of magnitude [14–16]. To date, this problem is not solvable with available computational resources.

Flavor evolution depends on the neutrino mixing parameters, as well as on the coherent forward scattering of neutrinos onto each other and on matter [9, 17–22]. Neutrino-neutrino interaction makes the equations of motion non-linear and correlates the flavor evolution of neutrinos of different momenta. A full solution of the quantum neutrino transport problem does not exist yet.

The omission of neutrino conversion in hydrodynamical simulations was not deemed worrisome as it was expected to occur beyond the shock radius, and thus, not having an impact on the shock revival [23]. However, this picture has been shaken by recent developments [24–28], hinting that neutrino conversion could already develop in the proximity of the neutrino decoupling region [29–39], with a characteristic time scale that is proportional to the number density of neutrinos and antineutrinos (hence

dubbed “fast” to distinguish it from the “slower” conversion driven by the vacuum frequency). The impact of flavor conversion on the supernova physics remains to be understood.

In the context of fast flavor conversion, an important role is played by the angular distributions of (anti)neutrinos: a crossing between the angular distributions of ν_e and $\bar{\nu}_e$, or a change of sign in the electron neutrino lepton number (ELN) within a certain angular range, constitutes a necessary condition to trigger a flavor instability [28, 40, 41], in the limit of vanishing mass-squared difference [16, 24, 26, 28, 30, 42–47]. The amount of induced flavor conversion is, however, unknown [48]. In the light of these developments, it becomes of paramount importance to ascertain whether the presence of ELN crossings is modified by flavor conversion and vice-versa.

In the supernova core, neutrinos are trapped with a mean-free path of $\mathcal{O}(10)$ m at typical baryon densities of $\mathcal{O}(10^{14})$ g/cm³ [49]. As the distance from the supernova increases and the baryon density decreases, neutrinos start decoupling from matter. However, not all flavors of neutrinos decouple simultaneously due to the flavor dependent cross section of neutrinos. Their angular distributions are initially almost isotropic and, as the density decreases, become forward peaked and ELN crossings can form, also because of collisions and advection [38, 50]. Recent work shows that, if flavor conversion should occur in the decoupling region, a non-trivial feedback between neutrino flavor transformations and collisions could take place [50–57]. Similarly, neutrino advection and the spatial dimensionality of the problem could also dynamically modify the conditions for flavor conversion [43, 58].

In this *Letter*, we present the first investigation of flavor conversion as the angular distributions of neutrinos evolve in the collisional regime and in the presence of neutrino advection. Our findings highlight that these processes cannot be disentangled.

Mean field equations of neutrinos.—For the sake of simplicity, we work in the two-flavor approximation,

i.e. in the (ν_e, ν_x) basis [44, 46, 59, 60]. The [anti]neutrino field is described through a 2×2 density matrix, $\rho(\vec{r}, \vec{p}, t)$ [$\bar{\rho}(\vec{r}, \vec{p}, t)$]. The diagonal elements of the density matrix (ρ_{ii} , with $i = e, x$) represent the occupation numbers of neutrinos of different species, while the off-diagonal terms (ρ_{ij}) encode flavor coherence. The evolution of the neutrino field at time t , location \vec{r} and momentum \vec{p} is governed by the following equation [61]:

$$\left(\frac{\partial}{\partial t} + \vec{v} \cdot \vec{\nabla} \right) \rho(\vec{r}, \vec{p}, t) = \mathcal{C} - i[H(\vec{r}, \vec{p}, t), \rho(\vec{r}, \vec{p}, t)]. \quad (1)$$

The term in parenthesis on the left-hand side of Eq. 1 is the total derivative. For simplicity, in the following we work in spherical symmetry and assume only one energy mode E ; hence, $\rho(\vec{r}, \vec{p}, t) = \rho(r, E, \theta, t)$, with θ being the local polar angle defined with respect to the radial direction and defined at a given r .

The commutator on the right hand side of Eq. 1 encodes the flavor evolution of neutrinos. The Hamiltonian, $H = H_{\text{vac}} + H_{\text{matt}} + H_{\nu\nu}$, governs the coherent evolution of neutrinos and is composed of the vacuum and neutrino self-interaction term:

$$H_{\text{vac}} = \frac{\omega}{2} \begin{pmatrix} -\cos 2\vartheta_V & \sin 2\vartheta_V \\ \sin 2\vartheta_V & \cos 2\vartheta_V \end{pmatrix}, \quad (2)$$

$$H_{\nu\nu} = \mu_0 \int [\rho(\cos \theta') - \bar{\rho}(\cos \theta')] \times (1 - \cos \theta \cos \theta') d \cos \theta', \quad (3)$$

where we have absorbed the constant factor coming from the integration over the azimuthal angle in μ_0 and suppressed the dependence on r and t for the sake of brevity. The term, H_{matt} , linked to matter effects should also appear in H . However, the effect of the matter potential is to suppress the vacuum mixing angle ϑ_V [62], hence we set $H_{\text{matt}} = 0$ and use $\vartheta_V = 10^{-3}$ instead. The vacuum frequency is $\omega = \Delta m^2 / 2E$, with Δm^2 being the squared mass difference. For antineutrinos, $\omega \rightarrow -\omega$ in H_{vac} , while all other terms of H remain unchanged.

The collision term in Eq. 1, $\mathcal{C} \equiv \mathcal{C}(\vec{r}, E, t) = \mathcal{C}_{\text{emission}} + \mathcal{C}_{\text{absorb}} + \mathcal{C}_{\text{dir-ch}}$, includes emission, absorption, and direction-changing collisions, respectively [63]. It encapsulates all the reactions of neutrinos with the matter background [6, 50, 64, 65]. We assume that the collision term only affects the diagonal components of the density matrices, as the time-scales associated with flavor evolution are shorter than the collision ones [16].

We rely on a heuristic collision term that allows for neutrinos to transition from the trapping regime to free streaming within a small spatial range (i.e., [15,30] km in our simulations), since we are limited by the size of our simulation box—due to technical complications induced by the treatment of flavor conversion. For simplicity, we retain the dependence of \mathcal{C} on r and neglect its angular dependence because it is dominated by the interaction of

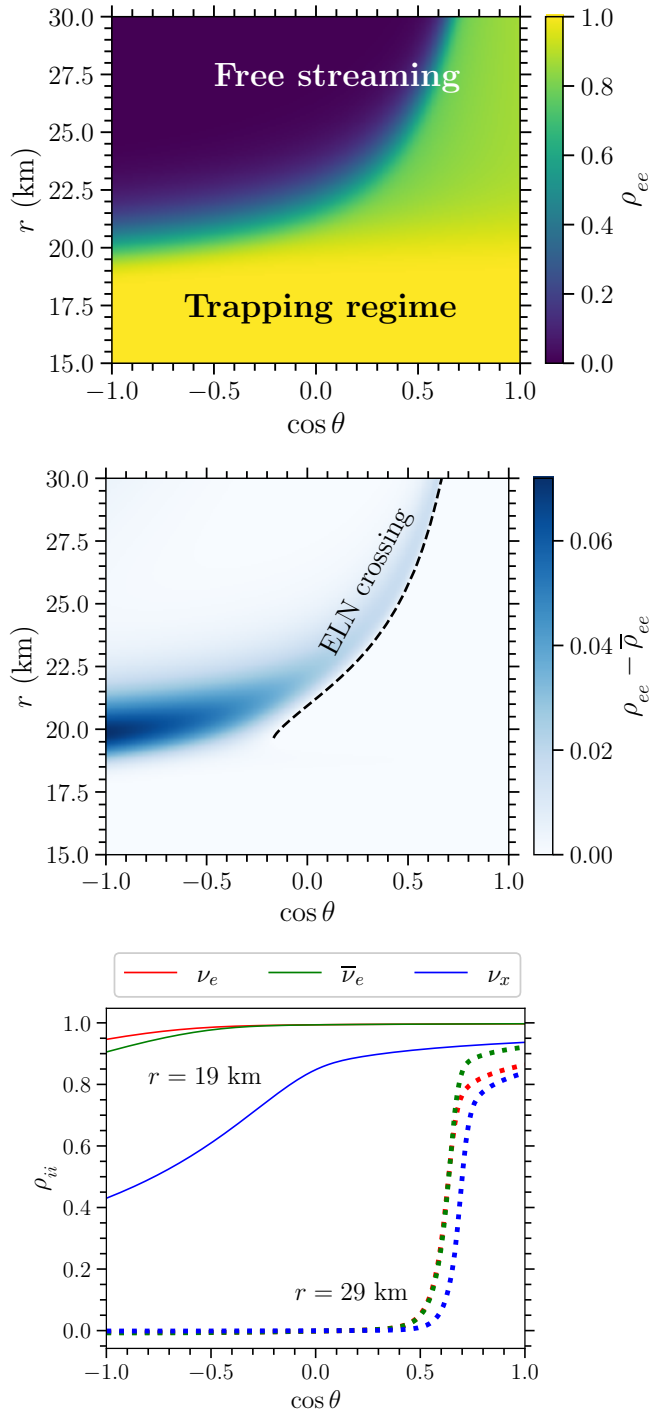


FIG. 1. Steady state neutrino flavor configuration in the absence of flavor mixing. These distributions (generated by imposing $H = 0$ in Eq. 1 and extracted at $t = 10^{-4}$ s) are the ones adopted as input to investigate the effects of flavor conversion. *Top panel:* Contour plot of ρ_{ee} (proportional to the ν_e number density) in the plane spanned by $\cos \theta$ and r . *Middle panel:* Same as in the top panel but for $\rho_{ee} - \bar{\rho}_{ee}$ (proportional to the ELN density). The dashed line marks the region where ELN crossings develop. *Bottom panel:* Angular distributions of ν_e , $\bar{\nu}_e$ and ν_x at $r = 19$ km (solid) and 29 km (dotted). As r increases, the angular distributions become prominently forward peaked in a flavor-dependent fashion and ELN crossings develop.

TABLE I. Inverse length-scales associated with emission, absorption and direction-changing scattering for all the flavors (see Eqs. 4–6). The function $\xi(r) = \exp(-(r - 15)/\text{km})$ ensures that the collision term vanishes at large distances.

	ν_e	$\bar{\nu}_e$	$\nu_x, \bar{\nu}_x$
$\lambda_{\text{emission}}^{\nu_i}$ (km ⁻¹)	1/50 $\xi(r)$	1/25 $\xi(r)$	1/10 $\xi(r)$
$\lambda_{\text{absorb}}^{\nu_i}$ (km ⁻¹)	1/50 $\xi(r)$	1/25 $\xi(r)$	1/10 $\xi(r)$
$\lambda_{\text{dir-ch}}^{\nu_i}$ (km ⁻¹)	1/50 $\xi(r)$	1/25 $\xi(r)$	1/12.5 $\xi(r)$

neutrinos with nucleons that are heavier than the neutrino average energies:

$$\mathcal{C}_{\text{emission}}^{\nu_e, \bar{\nu}_e, \nu_x, \bar{\nu}_x} = \frac{1}{\lambda_{\text{emission}}^{\nu_e, \bar{\nu}_e, \nu_x, \bar{\nu}_x}(r)}, \quad (4)$$

$$\mathcal{C}_{\text{absorb}}^{\nu_e, \bar{\nu}_e, \nu_x, \bar{\nu}_x} = -\frac{1}{\lambda_{\text{absorb}}^{\nu_e, \bar{\nu}_e, \nu_x, \bar{\nu}_x}(r)} \rho_{ii}(\cos \theta), \quad (5)$$

$$\begin{aligned} \mathcal{C}_{\text{dir-ch}}^{\nu_e, \bar{\nu}_e, \nu_x, \bar{\nu}_x} = & -\frac{2}{\lambda_{\text{dir-ch}}^{\nu_e, \bar{\nu}_e, \nu_x, \bar{\nu}_x}(r)} \rho_{ii}(\cos \theta) \\ & + \int_{-1}^1 \frac{1}{\lambda_{\text{dir-ch}}^{\nu_e, \bar{\nu}_e, \nu_x, \bar{\nu}_x}(r)} \rho_{ii}(\cos \theta') d \cos \theta'. \end{aligned} \quad (6)$$

Each of the above equations refers to all flavors as denoted by the superscripts, and the flavor-dependent length-scales, λ^{ν_i} , are tabulated in Table I and shown in Fig. S1 of the Supplemental Material. Equations 4 and 5 determine the rate at which neutrinos traveling in the direction θ are created and absorbed, respectively. Equation 6 represents the probability that a neutrino traveling along θ' will change to the θ direction. While Eqs. 4 and 5 do not conserve the number of neutrinos, Eq. 6 preserves the number of neutrinos.

In our simulations, neutrinos of all flavors are generated through collisions. The ratio between $\mathcal{C}_{\text{emission}}$ and $\mathcal{C}_{\text{absorb}}$ determines ρ_{ii} for all flavors at $r_{\text{min}} = 15$ km. Since only $\mathcal{C}_{\text{emission}}$ and $\mathcal{C}_{\text{absorb}}$ play a role in the trapping regime, the number density at r_{min} can be determined analytically in the steady state configuration. At larger r , $\mathcal{C}_{\text{dir-ch}}$ also comes into play in shaping the angular distributions and no analytical solution exists. In addition, in our simplified setup, we neglect Pauli blocking [66, 67] and assume that the neutrino chemical potentials are negligible.

In what follows, we first investigate the decoupling of neutrinos in the absence of flavor conversion and then we take into account flavor transformation. In order to do that, we focus on the simulation box from 15 to 30 km, resembling a box in the supernova core. We assume that neutrinos have $\omega = 0.32$ km⁻¹, which corresponds to $E = 20$ MeV for $\Delta m^2 = 2.5 \times 10^{-3}$ eV², and $\mu_0 = 10^4$ km⁻¹. Technical details on the numerical implementation of the problem will be reported in a separate publication [68].

Neutrino decoupling in the absence of neutrino flavor conversion.—The decoupling of neutrinos from matter is driven by the flavor-dependent collision term along with neutrino advection [50, 69]. Solving Eq. 1 for $H = 0$

(i.e. in the absence of flavor conversion) and no neutrinos in the simulation box at $t = 0$, the collision terms in Eqs. 4–6 lead to a steady state configuration for each neutrino species after a sufficiently large time interval ($t \gtrsim 10^{-4}$ s). The top panel of Fig. 1 shows a contour plot of ρ_{ee} in the plane spanned by $\cos \theta$ and r . At small radii, the angular distribution ($15 \lesssim r \lesssim 18$ km) is uniform in $\cos \theta$; as r increases, the angular distribution becomes gradually forward peaked and its backward part ($\cos \theta \lesssim 0$) is progressively emptied as full decoupling is reached. A similar behavior holds for all (anti)neutrino species. Despite the heuristic approach adopted to model the collision term, we find that ν_e 's have the smallest mean-free-path while non-electron type neutrinos have the longest mean-free path (see Supplemental Material), as expected [6, 64, 65]. Moreover, the ν_e decoupling radius is larger than the $\bar{\nu}_e$ one [70, 71].

As the presence of ELN crossings is crucial to the development of fast flavor conversion, the middle panel of Fig. 1 displays a contour of $\rho_{ee} - \bar{\rho}_{ee}$ in the plane spanned by $\cos \theta$ and r . ELN crossings are not prominent at small r , but they develop at $r \gtrsim 18$ km and affect different angular regions as r increases. The dark blue band to the left of the dashed line in Fig. 1 is the region with an excess of ν_e over $\bar{\nu}_e$ due to the fact that the $\bar{\nu}_e$ decoupling radius is smaller than the ν_e one. The bottom panel of Fig. 1 displays snapshots of the angular distributions of ν_e , $\bar{\nu}_e$, and $\nu_x = \bar{\nu}_x$ at two representative radii. As \mathcal{C} evolves as a function of r , the angular distribution of each flavor becomes forward peaked and ELN crossings are visible.

The dashed lines in the top panel of Fig. 2 show the radial evolution of the angle-averaged occupation number for ν_e and ν_x . In order to determine the decoupling surface, we compute the flux factor:

$$\mathcal{F}_{\nu_i} = \frac{\int_{-1}^1 \rho_{ii}(\cos \theta) \cos \theta d \cos \theta}{\int_{-1}^1 \rho_{ii}(\cos \theta) d \cos \theta}. \quad (7)$$

and approximately define the radius of decoupling as the radius at which the flux factor is $\mathcal{F}_{\nu_i} = 1/3$ [29, 72]. The corresponding decoupling surfaces of ν_e and ν_x are shown in the top panel of Fig. 2.

Neutrino decoupling in the presence of neutrino flavor conversion.—Switching on flavor mixing in Eq. 1 (i.e., $H \neq 0$), and adopting the steady state flavor configuration in Fig. 1 as the initial state, leads to fascinating insights into the effect of flavor conversion on neutrino decoupling. The solid lines in the top panel of Fig. 2 show the angle averaged occupation numbers of ν_e and ν_x . With respect to the case without mixing (dashed lines in Fig. 2), we see that flavor mixing pushes the distributions of ν_e and ν_x towards each other, sensibly modifying them with respect to the case without flavor conversion. However, we stress that flavor equipartition is not a general outcome, but it is linked to the specific flavor setup adopted in this paper; we have found other flavor config-

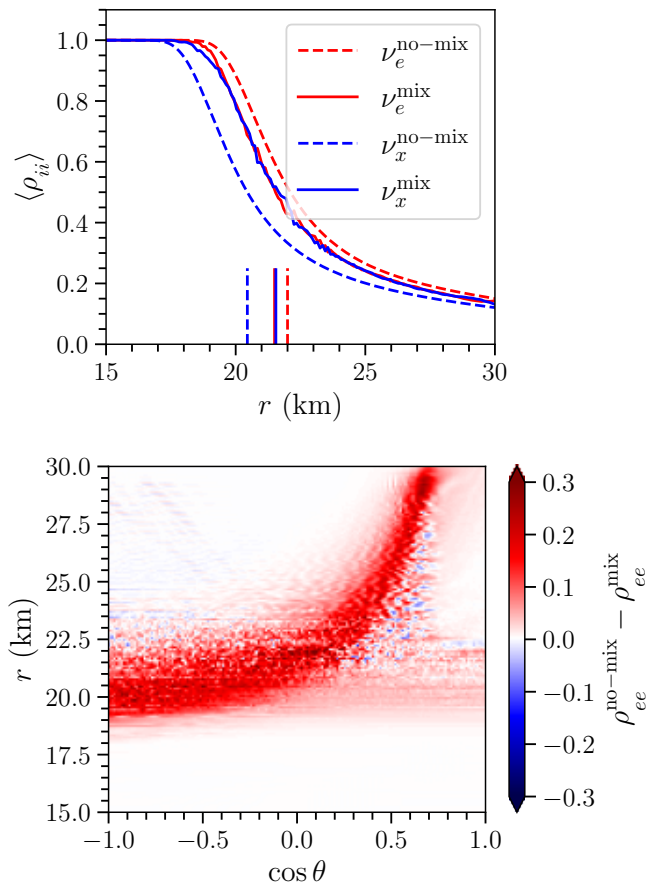


FIG. 2. Steady state neutrino flavor configuration in the presence of flavor mixing (extracted 5×10^{-5} s after the classical steady state configuration is reached in our simulation). *Top*: Angle averaged neutrino occupation numbers of ν_e (in red) and ν_x (in blue) with (solid lines) and without (dashed lines) neutrino mixing as functions of the radius. The vertical lines mark the radii of decoupling (approximately defined as the radius at which $\mathcal{F}_{\nu_i} = 1/3$). A similar trend holds for antineutrinos; however, note that flavor conversion induces a difference between ν_x and $\bar{\nu}_x$. *Bottom*: Contour plot of the difference between the ν_e occupation number without (when the classical steady state configuration is achieved) and with neutrino mixing in the plane spanned by $\cos \theta$ and r . The red regions indicate a ν_e deficit due to flavor conversion, while the small islands in blue represent an excess of ν_e due to neutrino conversion. The mixture between blue and red spots is the result of the interplay between collisions and advection. Due to the collective nature of the neutrino flavor evolution and flavor lepton number conservation, the corresponding heatmap for antineutrinos looks very similar and is not shown.

urations that do not lead to flavor equipartition (results not shown here), see also Ref. [73]. The impact of neutrino flavor evolution is evident in the shift of the radius at which the angle-averaged ρ_{ee} and ρ_{xx} start falling, with consequences on the decoupling radius.

Interestingly, despite the presence of ELN crossings (see middle panel of Fig. 1) only a small radial range

centered on $r \simeq 21$ km is affected by flavor instabilities in the limit of $\omega = 0$ (i.e., when only fast conversion occurs). This implies that the non-trivial angular distributions due to the interplay between the advective term and collisions and $\omega \neq 0$ are responsible for triggering slow collective neutrino transformations at high densities, in contrast to what is commonly assumed in the literature; the growth rate of the flavor instabilities is shown in Fig. S3 of the Supplemental Material.

One of the consequences of neutrino flavor conversion is a shift in the radius of neutrino decoupling. The top panel of Fig. 2 shows the flavor dependent decoupling surfaces with (solid) and without (dashed) mixing for comparison. It is also important to note that neutrinos start to change their flavor at radii much smaller than their decoupling surfaces; this is in stark contrast with the approximation of flavor-independent neutrinosphere commonly adopted in the literature [14, 15, 18–21], under the naive expectation that flavor evolution near the neutrinosphere would not be present due to collisional damping [74–76].

The bottom panel of Fig. 2 represents the difference in the ν_e occupation number in the absence and presence of neutrino mixing. As r increases, a region with a deficit of ν_e forms due to flavor conversion (red band). Because of the interplay with collisions and advection, the red band is flanked by small blue islands where the opposite takes place. This effect cannot be captured by any calculation that does not include advection and collision, together with flavor transformation—see Fig. S4 and the animations in the Supplemental Material for comparison.

Outlook.—For the first time, we follow the flavor evolution while neutrinos decouple, in the presence of collisions and advection in spherical symmetry. We find that neutrino flavor conversion occurs well before all flavors decouple from the matter background and the neutrino decoupling surfaces are affected by flavor transformation.

While dealing with flavor transformation, advection and collisions simultaneously for the first time, the collision term adopted in this work relies on heuristic functions that allow us to transition from uniform to forward peaked neutrino distributions within a small spatial region because of the technical challenges induced by the treatment of flavor conversion in the stellar core. A further exacerbation of our findings could be due to the inclusion of all six flavors, the energy dependence of the neutrino distributions, and the azimuthal emission angle of neutrinos [42, 44, 58–60, 77]. Additional effects on the decoupling physics may arise from relaxing the assumption of spatial homogeneity [78]. Not only can spatial inhomogeneity lead to additional flavor instabilities, neutrino advection causes dynamical effects which can only manifest in an inhomogeneous system [43].

Despite its caveats, this work clearly demonstrates that the neutrino decoupling physics is affected by flavor transformation, with possible implications on the neu-

trino energy deposition in the supernova gain layer that remain to be assessed. The fact that the dynamics of neutrino decoupling changes due to neutrino flavor transformation implies that the neutrino properties at the radius of decoupling may be different from the ones usually computed in hydrodynamic simulations treating neutrinos as radiation. However, a robust assessment of the radiated neutrino spectra in the presence of flavor conversion will have to take into account the hydrodynamic feedback on the thermodynamic properties of the proto-neutron star. The occurrence of flavor conversion in the vicinity of the flavor-dependent neutrinospheres puts in perspective the existing literature naively assuming flavor-independent neutrinospheres and a larger radius for the onset of flavor conversion. Our findings may also have implications in the context of compact binary merger remnants. In fact, the possible impact of neutrino flavor conversion on the synthesis of the heavy elements and the related kilonova lightcurve is yet to be determined [72, 79–83].

Acknowledgments.—We thank Eve Armstrong, Rasmus S. L. Hansen, Christopher Rackauckas, and Anna Suliga for useful discussions, as well as Thomas Janka and Georg Raffelt for insightful feedback on the manuscript. We are grateful to the Villum Foundation (Project No. 13164), the Danmarks Frie Forskningsfonds (Project No. 8049-00038B), the MERAC Foundation, and the Deutsche Forschungsgemeinschaft through Sonderforschungsbereich SFB 1258 “Neutrinos and Dark Matter in Astro- and Particle Physics” (NDM).

-
- [1] A. Burrows and D. Vartanyan, Core-Collapse Supernova Explosion Theory, *Nature* **589**, 29 (2021), arXiv:2009.14157 [astro-ph.SR].
- [2] H.-T. Janka, T. Melson, and A. Summa, Physics of Core-Collapse Supernovae in Three Dimensions: a Sneak Preview, *Ann. Rev. Nucl. Part. Sci.* **66**, 341 (2016), arXiv:1602.05576 [astro-ph.SR].
- [3] S. A. Colgate and R. H. White, The Hydrodynamic Behavior of Supernovae Explosions, *Astrophys. J.* **143**, 626 (1966).
- [4] J. R. Wilson, Supernovae and Post-Collapse Behavior, in *Numerical Astrophysics* (1985) p. 422.
- [5] H. A. Bethe and J. R. Wilson, Revival of a stalled supernova shock by neutrino heating, *Astrophys. J.* **295**, 14 (1985).
- [6] A. Mezzacappa, E. Endeve, O. E. B. Messer, and S. W. Bruenn, Physical, numerical, and computational challenges of modeling neutrino transport in core-collapse supernovae, (2020), arXiv:2010.09013 [astro-ph.HE].
- [7] A. Burrows, D. Vartanyan, J. C. Dolence, M. A. Skinner, and D. Radice, Crucial Physical Dependencies of the Core-Collapse Supernova Mechanism, *Space Sci. Rev.* **214**, 33 (2018), arXiv:1611.05859 [astro-ph.SR].
- [8] D. Mihalas and B. Mihalas, Book-Review - Foundations of Radiation Hydrodynamics, *Sky & Telescope* **70**, 231 (1985).
- [9] G. Sigl and G. G. Raffelt, General kinetic description of relativistic mixed neutrinos, *Nucl. Phys. B* **406**, 423 (1993).
- [10] A. Vlasenko, G. M. Fuller, and V. Cirigliano, Neutrino Quantum Kinetics, *Phys. Rev. D* **89**, 105004 (2014), arXiv:1309.2628 [hep-ph].
- [11] A. Vlasenko, G. M. Fuller, and V. Cirigliano, Prospects for Neutrino-Antineutrino Transformation in Astrophysical Environments, (2014), arXiv:1406.6724 [astro-ph.HE].
- [12] J. Serreau and C. Volpe, Neutrino-antineutrino correlations in dense anisotropic media, *Phys. Rev. D* **90**, 125040 (2014), arXiv:1409.3591 [hep-ph].
- [13] D. N. Blaschke and V. Cirigliano, Neutrino Quantum Kinetic Equations: The Collision Term, *Phys. Rev. D* **94**, 033009 (2016), arXiv:1605.09383 [hep-ph].
- [14] H. Duan, G. M. Fuller, and Y.-Z. Qian, Collective Neutrino Oscillations, *Ann. Rev. Nucl. Part. Sci.* **60**, 569 (2010), arXiv:1001.2799 [hep-ph].
- [15] A. Mirizzi, I. Tamborra, H.-T. Janka, N. Saviano, K. Scholberg, R. Bollig, L. Hüdepohl, and S. Chakraborty, Supernova Neutrinos: Production, Oscillations and Detection, *Riv. Nuovo Cim.* **39**, 1 (2016), arXiv:1508.00785 [astro-ph.HE].
- [16] I. Tamborra and S. Shalgar, New Developments in Flavor Evolution of a Dense Neutrino Gas, *Ann. Rev. Nucl. Part. Sci.* **71**, 165 (2021), arXiv:2011.01948 [astro-ph.HE].
- [17] J. T. Pantaleone, Neutrino oscillations at high densities, *Phys. Lett. B* **287**, 128 (1992).
- [18] H. Duan, G. M. Fuller, and Y.-Z. Qian, Collective neutrino flavor transformation in supernovae, *Phys. Rev. D* **74**, 123004 (2006), arXiv:astro-ph/0511275 [astro-ph].
- [19] H. Duan, G. M. Fuller, J. Carlson, and Y.-Z. Qian, Simulation of Coherent Non-Linear Neutrino Flavor Transformation in the Supernova Environment. 1. Correlated Neutrino Trajectories, *Phys. Rev. D* **74**, 105014 (2006), arXiv:astro-ph/0606616 [astro-ph].
- [20] H. Duan, G. M. Fuller, J. Carlson, and Y.-Z. Qian, Coherent Development of Neutrino Flavor in the Supernova Environment, *Phys. Rev. Lett.* **97**, 241101 (2006), arXiv:astro-ph/0608050 [astro-ph].
- [21] G. Fogli, E. Lisi, A. Marrone, and A. Mirizzi, Collective neutrino flavor transitions in supernovae and the role of trajectory averaging, *JCAP* **0712**, 010, arXiv:0707.1998 [hep-ph].
- [22] S. Hannestad, G. G. Raffelt, G. Sigl, and Y. Y. Y. Wong, Self-induced conversion in dense neutrino gases: Pendulum in flavour space, *Phys. Rev. D* **74**, 105010 (2006), [Erratum: *Phys.Rev.D* 76, 029901 (2007)], arXiv:astro-ph/0608695.
- [23] B. Dasgupta, E. P. O’Connor, and C. D. Ott, The Role of Collective Neutrino Flavor Oscillations in Core-Collapse Supernova Shock Revival, *Phys. Rev. D* **85**, 065008 (2012), arXiv:1106.1167 [astro-ph.SR].
- [24] R. F. Sawyer, Speed-up of neutrino transformations in a supernova environment, *Phys. Rev. D* **72**, 045003 (2005), arXiv:hep-ph/0503013.
- [25] R. F. Sawyer, The multi-angle instability in dense neutrino systems, *Phys. Rev. D* **79**, 105003 (2009), arXiv:0803.4319 [astro-ph].
- [26] R. F. Sawyer, Neutrino cloud instabilities just above the neutrino sphere of a supernova, *Phys. Rev. Lett.* **116**, 081101 (2016), arXiv:1509.03323 [astro-ph.HE].
- [27] S. Chakraborty, R. S. Hansen, I. Izaguirre, and G. G.

- Raffelt, Self-induced neutrino flavor conversion without flavor mixing, *JCAP* **03**, 042, arXiv:1602.00698 [hep-ph].
- [28] I. Izaguirre, G. G. Raffelt, and I. Tamborra, Fast Pairwise Conversion of Supernova Neutrinos: A Dispersion-Relation Approach, *Phys. Rev. Lett.* **118**, 021101 (2017), arXiv:1610.01612 [hep-ph].
- [29] I. Tamborra, L. Hüdepohl, G. G. Raffelt, and H.-T. Janka, Flavor-dependent neutrino angular distribution in core-collapse supernovae, *Astrophys. J.* **839**, 132 (2017), arXiv:1702.00060 [astro-ph.HE].
- [30] S. Abbar, H. Duan, K. Sumiyoshi, T. Takiwaki, and M. C. Volpe, On the occurrence of fast neutrino flavor conversions in multidimensional supernova models, *Phys. Rev.* **D100**, 043004 (2019), arXiv:1812.06883 [astro-ph.HE].
- [31] M. Delfan Azari, S. Yamada, T. Morinaga, W. Iwakami, H. Okawa, H. Nagakura, and K. Sumiyoshi, Linear Analysis of Fast-Pairwise Collective Neutrino Oscillations in Core-Collapse Supernovae based on the Results of Boltzmann Simulations, *Phys. Rev. D* **99**, 103011 (2019), arXiv:1902.07467 [astro-ph.HE].
- [32] T. Morinaga, H. Nagakura, C. Kato, and S. Yamada, Fast neutrino-flavor conversion in the preshock region of core-collapse supernovae, *Physical Review Research* **2**, 012046 (2020), arXiv:1909.13131 [astro-ph.HE].
- [33] M. Delfan Azari, S. Yamada, T. Morinaga, H. Nagakura, S. Furusawa, A. Harada, H. Okawa, W. Iwakami, and K. Sumiyoshi, Fast collective neutrino oscillations inside the neutrino sphere in core-collapse supernovae, *Phys. Rev. D* **101**, 023018 (2020), arXiv:1910.06176 [astro-ph.HE].
- [34] H. Nagakura, T. Morinaga, C. Kato, and S. Yamada, Fast-pairwise Collective Neutrino Oscillations Associated with Asymmetric Neutrino Emissions in Core-collapse Supernovae, *Astrophys. J.* **886**, 139 (2019), arXiv:1910.04288 [astro-ph.HE].
- [35] S. Abbar, H. Duan, K. Sumiyoshi, T. Takiwaki, and M. C. Volpe, Fast Neutrino Flavor Conversion Modes in Multidimensional Core-collapse Supernova Models: the Role of the Asymmetric Neutrino Distributions, *Phys. Rev. D* **101**, 043016 (2020), arXiv:1911.01983 [astro-ph.HE].
- [36] R. Glas, H.-T. Janka, F. Capozzi, M. Sen, B. Dasgupta, A. Mirizzi, and G. Sigl, Fast Neutrino Flavor Instability in the Neutron-star Convection Layer of Three-dimensional Supernova Models, *Phys. Rev. D* **101**, 063001 (2020), arXiv:1912.00274 [astro-ph.HE].
- [37] F. Capozzi, S. Abbar, R. Bollig, and H.-T. Janka, Fast neutrino flavor conversions in one-dimensional core-collapse supernova models with and without muon creation, *Phys. Rev. D* **103**, 063013 (2021), arXiv:2012.08525 [astro-ph.HE].
- [38] H. Nagakura, L. Johns, A. Burrows, and G. M. Fuller, Where, when, and why: Occurrence of fast-pairwise collective neutrino oscillation in three-dimensional core-collapse supernova models, *Phys. Rev. D* **104**, 083025 (2021), arXiv:2108.07281 [astro-ph.HE].
- [39] A. Harada and H. Nagakura, Prospects of Fast Flavor Neutrino Conversion in Rotating Core-collapse Supernovae, *Astrophys. J.* **924**, 109 (2022), arXiv:2110.08291 [astro-ph.HE].
- [40] T. Morinaga, Fast neutrino flavor instability and neutrino flavor lepton number crossings, *Phys. Rev. D* **105**, L101301 (2022), arXiv:2103.15267 [hep-ph].
- [41] B. Dasgupta, Collective Neutrino Flavor Instability Requires a Crossing, *Phys. Rev. Lett.* **128**, 081102 (2022), arXiv:2110.00192 [hep-ph].
- [42] S. Shalgar and I. Tamborra, Dispelling a myth on dense neutrino media: fast pairwise conversions depend on energy, *JCAP* **01**, 014, arXiv:2007.07926 [astro-ph.HE].
- [43] S. Shalgar, I. Padilla-Gay, and I. Tamborra, Neutrino propagation hinders fast pairwise flavor conversions, *JCAP* **06**, 048, arXiv:1911.09110 [astro-ph.HE].
- [44] S. Shalgar and I. Tamborra, Three flavor revolution in fast pairwise neutrino conversion, *Phys. Rev. D* **104**, 023011 (2021), arXiv:2103.12743 [hep-ph].
- [45] L. Johns, H. Nagakura, G. M. Fuller, and A. Burrows, Neutrino oscillations in supernovae: angular moments and fast instabilities, *Phys. Rev. D* **101**, 043009 (2020), arXiv:1910.05682 [hep-ph].
- [46] M. Chakraborty and S. Chakraborty, Three flavor neutrino conversions in supernovae: slow & fast instabilities, *JCAP* **01**, 005, arXiv:1909.10420 [hep-ph].
- [47] B. Dasgupta, A. Mirizzi, and M. Sen, Fast neutrino flavor conversions near the supernova core with realistic flavor-dependent angular distributions, *JCAP* **02**, 019, arXiv:1609.00528 [hep-ph].
- [48] I. Padilla-Gay, I. Tamborra, and G. G. Raffelt, Neutrino Flavor Pendulum Reloaded: The Case of Fast Pairwise Conversion, *Phys. Rev. Lett.* **128**, 121102 (2022), arXiv:2109.14627 [astro-ph.HE].
- [49] G. E. Brown, H. A. Bethe, and G. Baym, Supernova theory, *Nucl. Phys. A* **375**, 481 (1982).
- [50] S. Shalgar and I. Tamborra, On the Occurrence of Crossings Between the Angular Distributions of Electron Neutrinos and Antineutrinos in the Supernova Core, *Astrophys. J.* **883**, 80 (2019), arXiv:1904.07236 [astro-ph.HE].
- [51] S. Shalgar and I. Tamborra, A change of direction in pairwise neutrino conversion physics: The effect of collisions, *Phys. Rev. D* **103**, 063002 (2021), arXiv:2011.00004 [astro-ph.HE].
- [52] R. S. L. Hansen, S. Shalgar, and I. Tamborra, Collisional dilemma: Enhancement or damping of fast flavor conversion of neutrinos, (2022), arXiv:2204.11873 [astro-ph.HE].
- [53] H. Sasaki and T. Takiwaki, Dynamics of fast neutrino flavor conversions with scattering effects: a detailed analysis, (2021), arXiv:2109.14011 [hep-ph].
- [54] J. D. Martin, J. Carlson, V. Cirigliano, and H. Duan, Fast flavor oscillations in dense neutrino media with collisions, *Phys. Rev. D* **103**, 063001 (2021), arXiv:2101.01278 [hep-ph].
- [55] F. Capozzi, B. Dasgupta, A. Mirizzi, M. Sen, and G. Sigl, Collisional triggering of fast flavor conversions of supernova neutrinos, *Phys. Rev. Lett.* **122**, 091101 (2019), arXiv:1808.06618 [hep-ph].
- [56] L. Johns, Collisional flavor instabilities of supernova neutrinos, (2021), arXiv:2104.11369 [hep-ph].
- [57] S. A. Richers, G. C. McLaughlin, J. P. Kneller, and A. Vlasenko, Neutrino Quantum Kinetics in Compact Objects, *Phys. Rev. D* **99**, 123014 (2019), arXiv:1903.00022 [astro-ph.HE].
- [58] S. Richers, D. Willcox, and N. Ford, Neutrino fast flavor instability in three dimensions, *Phys. Rev. D* **104**, 103023 (2021), arXiv:2109.08631 [astro-ph.HE].
- [59] F. Capozzi, M. Chakraborty, S. Chakraborty, and M. Sen, Fast flavor conversions in supernovae: the rise of mu-tau neutrinos, *Phys. Rev. Lett.* **125**, 251801 (2020),

- arXiv:2005.14204 [hep-ph].
- [60] F. Capozzi, M. Chakraborty, S. Chakraborty, and M. Sen, Supernova Fast Flavor Conversions in 1+1 D : Influence of Mu-tau neutrinos, (2022), arXiv:2205.06272 [hep-ph].
- [61] G. Sigl and G. G. Raffelt, General kinetic description of relativistic mixed neutrinos, Nucl. Phys. B **406**, 423 (1993).
- [62] A. Esteban-Pretel, A. Mirizzi, S. Pastor, R. Tomas, G. G. Raffelt, P. D. Serpico, and G. Sigl, Role of dense matter in collective supernova neutrino transformations, Phys. Rev. D **78**, 085012 (2008), arXiv:0807.0659 [astro-ph].
- [63] S. Weinberg, *Lectures on Astrophysics* (Cambridge University Press, 2019).
- [64] R. L. Bowers and J. R. Wilson, A numerical model for stellar core collapse calculations., Astrophys. J. Suppl. **50**, 115 (1982).
- [65] E. O'Connor, An Open-Source Neutrino Radiation Hydrodynamics Code for Core-Collapse Supernovae, Astrophys. J. Suppl. **219**, 24 (2015), arXiv:1411.7058 [astro-ph.HE].
- [66] S. W. Bruenn, Stellar core collapse - Numerical model and infall epoch, Astrophys. J. Suppl. **58**, 771 (1985).
- [67] G. G. Raffelt, *Stars as laboratories for fundamental physics: The astrophysics of neutrinos, axions, and other weakly interacting particles* (1996).
- [68] S. Shalgar and I. Tamborra, in preparation, (2022).
- [69] C. D. Ott, A. Burrows, L. Dessart, and E. Livne, 2D Multi-Angle, Multi-Group Neutrino Radiation-Hydrodynamic Simulations of Postbounce Supernova Cores, Astrophys. J. **685**, 1069 (2008), arXiv:0804.0239 [astro-ph].
- [70] M. T. Keil, G. G. Raffelt, and H.-T. Janka, Monte Carlo study of supernova neutrino spectra formation, Astrophys. J. **590**, 971 (2003), arXiv:astro-ph/0208035.
- [71] G. G. Raffelt, M. T. Keil, R. Buras, H.-T. Janka, and M. Rampp, Supernova neutrinos: Flavor-dependent fluxes and spectra, in *4th Workshop on Neutrino Oscillations and their Origin (NOON2003)* (2003) pp. 380–387, arXiv:astro-ph/0303226.
- [72] M.-R. Wu, I. Tamborra, O. Just, and H.-T. Janka, Imprints of neutrino-pair flavor conversions on nucleosynthesis in ejecta from neutron-star merger remnants, Phys. Rev. D **96**, 123015 (2017), arXiv:1711.00477 [astro-ph.HE].
- [73] M.-R. Wu, M. George, C.-Y. Lin, and Z. Xiong, Collective fast neutrino flavor conversions in a 1D box: Initial conditions and long-term evolution, Phys. Rev. D **104**, 103003 (2021), arXiv:2108.09886 [hep-ph].
- [74] L. Stodolsky, Neutron Optics and Weak Currents, Phys. Lett. B **50**, 352 (1974).
- [75] R. A. Harris and L. Stodolsky, Two State Systems in Media and ‘Turing’s Paradox’, Phys. Lett. B **116**, 464 (1982).
- [76] L. Stodolsky, On the Treatment of Neutrino Oscillations in a Thermal Environment, Phys. Rev. D **36**, 2273 (1987).
- [77] S. Shalgar and I. Tamborra, Symmetry breaking induced by pairwise conversion of neutrinos in compact sources, Phys. Rev. D **105**, 043018 (2022), arXiv:2106.15622 [hep-ph].
- [78] H. Duan and S. Shalgar, Flavor instabilities in the neutrino line model, Phys. Lett. **B747**, 139 (2015), arXiv:1412.7097 [hep-ph].
- [79] M.-R. Wu and I. Tamborra, Fast neutrino conversions: Ubiquitous in compact binary merger remnants, Phys. Rev. D **95**, 103007 (2017), arXiv:1701.06580 [astro-ph.HE].
- [80] I. Padilla-Gay, S. Shalgar, and I. Tamborra, Multi-Dimensional Solution of Fast Neutrino Conversions in Binary Neutron Star Merger Remnants, JCAP **01**, 017, arXiv:2009.01843 [astro-ph.HE].
- [81] M. George, M.-R. Wu, I. Tamborra, R. Ardevol-Pulpillo, and H.-T. Janka, Fast neutrino flavor conversion, ejecta properties, and nucleosynthesis in newly-formed hypermassive remnants of neutron-star mergers, Phys. Rev. D **102**, 103015 (2020), arXiv:2009.04046 [astro-ph.HE].
- [82] O. Just, S. Abbar, M.-R. Wu, I. Tamborra, H.-T. Janka, and F. Capozzi, Fast neutrino conversion in hydrodynamic simulations of neutrino-cooled accretion disks, Phys. Rev. D **105**, 083024 (2022), arXiv:2203.16559 [astro-ph.HE].
- [83] X. Li and D. M. Siegel, Neutrino Fast Flavor Conversions in Neutron-Star Postmerger Accretion Disks, Phys. Rev. Lett. **126**, 251101 (2021), arXiv:2103.02616 [astro-ph.HE].
- [84] A. Banerjee, A. Dighe, and G. G. Raffelt, Linearized flavor-stability analysis of dense neutrino streams, Phys. Rev. D **84**, 053013 (2011), arXiv:1107.2308 [hep-ph].
- [85] V. Cirigliano, M. W. Paris, and S. Shalgar, Effect of collisions on neutrino flavor inhomogeneity in a dense neutrino gas, Phys. Lett. B **774**, 258 (2017), arXiv:1706.07052 [hep-ph].

Supplemental Material

Supernova Neutrino Decoupling Is Altered by Flavor Conversion

In this Supplemental Material, we expand on the modeling of the collision term in the neutrino equations of motion and provide additional details to characterize the interplay between flavor mixing, collisions, and advection. The flavor instabilities giving rise to flavor mixing in our simulations are a mixture of slow and fast conversions; we show this here by means of the linear stability analysis.

A. Neutrino interaction rates and neutrino densities

The flavor configuration displayed in Fig. 1 represents the classical steady state configuration obtained in the absence of neutrino flavor transformation. Within our setup, the neutrino angular distributions are populated through the effects of collisions and advection across the simulation box.

The radial profiles for the heuristic collision terms are shown in Fig. S1 (see also Table I). We can see that $\lambda_{\text{dir-ch}}^{-1}$ is the largest contribution for all flavors at small radii. As the radius increases, all inverse length-scales decrease, until they are negligible for $r \gtrsim 25$ km, when

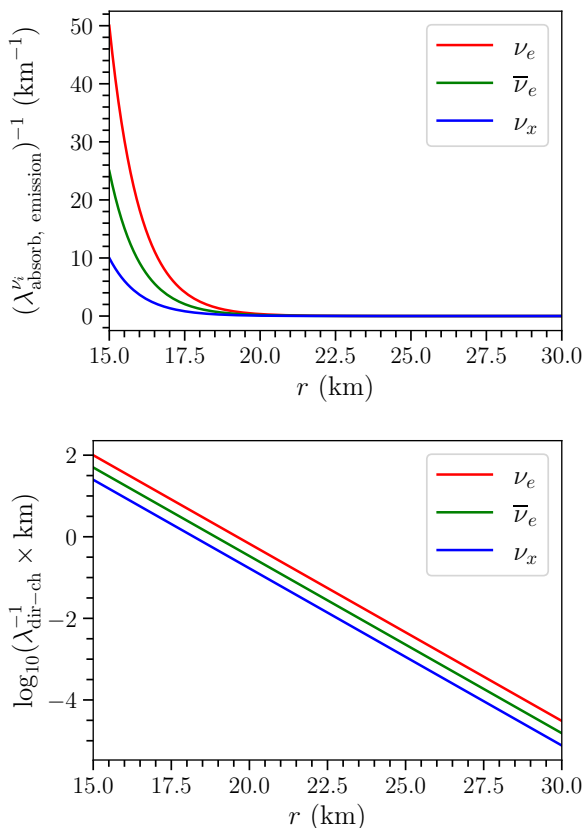


FIG. S1. Inverse length-scales associated with emission, absorption, and direction-changing scattering for ν_e (in red), $\bar{\nu}_e$ (in green), and ν_x (in blue) as functions of radius. The functional forms of these terms are reported in Table I, see also Eqs. 4–6.

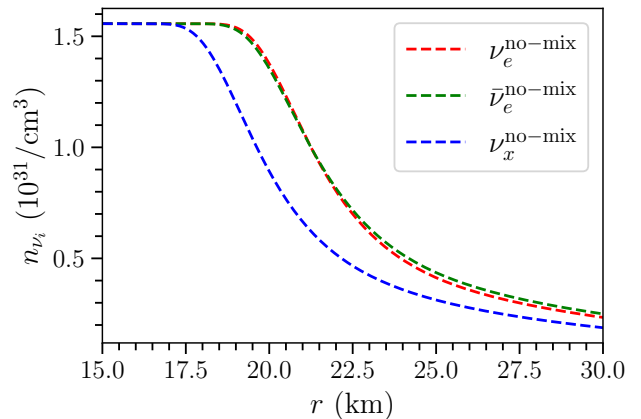


FIG. S2. Neutrino number densities of ν_e (in red), $\bar{\nu}_e$ (in green) and ν_x (in blue) as functions of radius in the steady state configuration in the absence of neutrino mixing. The number density has no radial dependence in the trapping regime ($r \lesssim 18$ km), while it falls off like $1/r^2$ at larger radii ($r \gtrsim 25$ km), as expected because the absorption and emission terms are very small.

neutrinos decouple from matter as shown in the top panel of Fig. 1. The fact that the $\bar{\nu}_e$ mean free path is larger than the ν_e one ensures that the $\bar{\nu}_e$'s decouple at a smaller radius than ν_e 's.

As neutrinos start to decouple from matter, the angular distribution for each neutrino flavor becomes forward peaked and the number density which is proportional to the diagonal components of the density matrix falls off. This is clearly visible from the radial profile of the number density for each flavor [which corresponds to $n_{\nu_i} = \mu_0 \rho_{ii} / (\sqrt{2} G_F)$ in physical units] shown in Fig. S2, in the steady state configuration and in the absence of neutrino mixing. At radii larger than ~ 25 km, the emission and absorption terms are almost zero. In this limit we find that the neutrino number density falls off like $1/r^2$ as expected due to conservation of neutrino number for each flavor. Also, since there is almost no absorption or emission of neutrinos in the region of $r \gtrsim 25$ km, the angular distributions become forward peaked as the only neutrinos that are present at these radii are the ones which have escaped the core and travel along directions that are close to the radial one.

B. Interplay between slow and fast flavor instabilities

The linear stability analysis consists of linearizing the equations of motion and calculating the growth rate of the flavor instability [84]. By setting the collision and the advective terms to zero ($\vec{v} = 0$), expanding Eq. 1 in the off-diagonal component, and ignoring $\mathcal{O}(\rho_{ex}^2)$ and higher order terms, the solutions are of the form:

$$\rho_{ex}(\cos \theta, t) \sim \exp(-i\Omega t)\rho_{ex}(\cos \theta, 0) \quad (\text{S1})$$

$$\bar{\rho}_{ex}(\cos \theta, t) \sim \exp(-i\Omega t)\bar{\rho}_{ex}(\cos \theta, 0). \quad (\text{S2})$$

The collective nature of flavor evolution ensures that the eigenvalue Ω is the same for neutrinos and antineutrinos and also the same for all values of $\cos \theta$. When a flavor instability is present, Ω has a positive imaginary component, called growth rate and denoted by κ . It should be noted that, although the complex eigenvalues are always present in complex conjugate pairs in the absence of the collision term, this is not the case in the presence of collisions [85]; which however we do not consider here. It should be noted, however, that the presence of neutrino flavor instability does not necessarily imply significant flavor transformation [80].

Figure S3 shows the growth rate as a function of radius for $\omega = 0$ (fast conversion) and $\omega = 0.32 \text{ km}^{-1}$ adopted in our work. Interestingly, for most of the radial range, the neutrino flavor instability does not exist for $\omega = 0$, implying that initially the neutrino flavor evolution is not driven by ELN crossings, but by the vacuum term. Fast flavor instabilities are only present in a small radial range around $\sim 21 \text{ km}$. In addition, once triggered, fast flavor mixing is further affected by the vacuum fre-

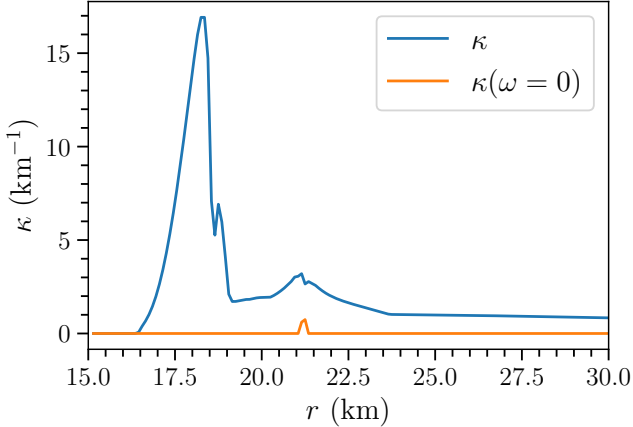


FIG. S3. Growth rate of the flavor instability as a function of radius obtained by adopting the steady state flavor distributions. The orange line shows the growth rate for $\omega = 0$ (fast conversion), whereas the blue line shows the growth for $\omega = 0.32 \text{ km}^{-1}$ (slow conversion). Contrary to expectations, flavor mixing is induced by slow instabilities; fast flavor instabilities are only present around $\sim 21 \text{ km}$.

quency [42]. By comparing Fig. S3 with Figs. S4 and 2, we note that although the neutrino flavor instability exists for $r \gtrsim 18 \text{ km}$, the magnitude of the neutrino flavor transformation is not directly correlated to κ , in agreement with the findings of Ref. [80] in the context of fast flavor transformation.

C. Dynamical effects and neutrino flavor conversion

After obtaining a steady state configuration for all flavors (see Fig. 1), we switch on flavor mixing and explore its interplay with neutrino advection and collisions. In order to highlight the dynamical effects of neutrino advection and collisions on flavor conversion, we show in Fig. S4 the correspondent flavor outcome obtained by switching off collisions and advection once the steady

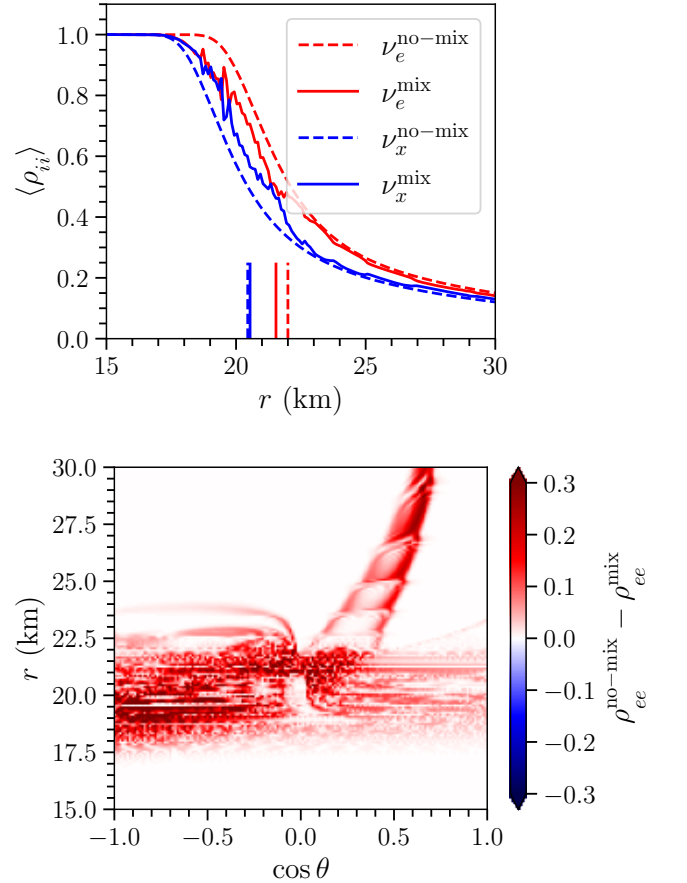


FIG. S4. Final flavor configuration obtained by switching on flavor mixing, after the classical steady state is reached, and switching off collisions and neutrino advection (i.e., $H \neq 0$, $C = 0$, and $\vec{v} = 0$ in Eq. 1). The top and bottom panels are the analogous of the ones in Fig. 2, which instead take into account the dynamical effects on flavor mixing due to collisions and advection (i.e., $H \neq 0$, $C \neq 0$, and $\vec{v} \neq 0$ in Eq. 1).

state flavor configuration is achieved, i.e. by letting flavor transformation operate in the absence of collisions and advection.

Figure S4 should be compared with Fig. 2. One can see that collisions and neutrino advection non only affect the final angle-integrated flavor configuration, but also allow to spread the flavor instabilities across angular regions and spatial ranges [43, 51, 52]. It is also worth noticing that the absence of neutrino advection makes the evolution of neutrino flavor much more oscillatory in nature.